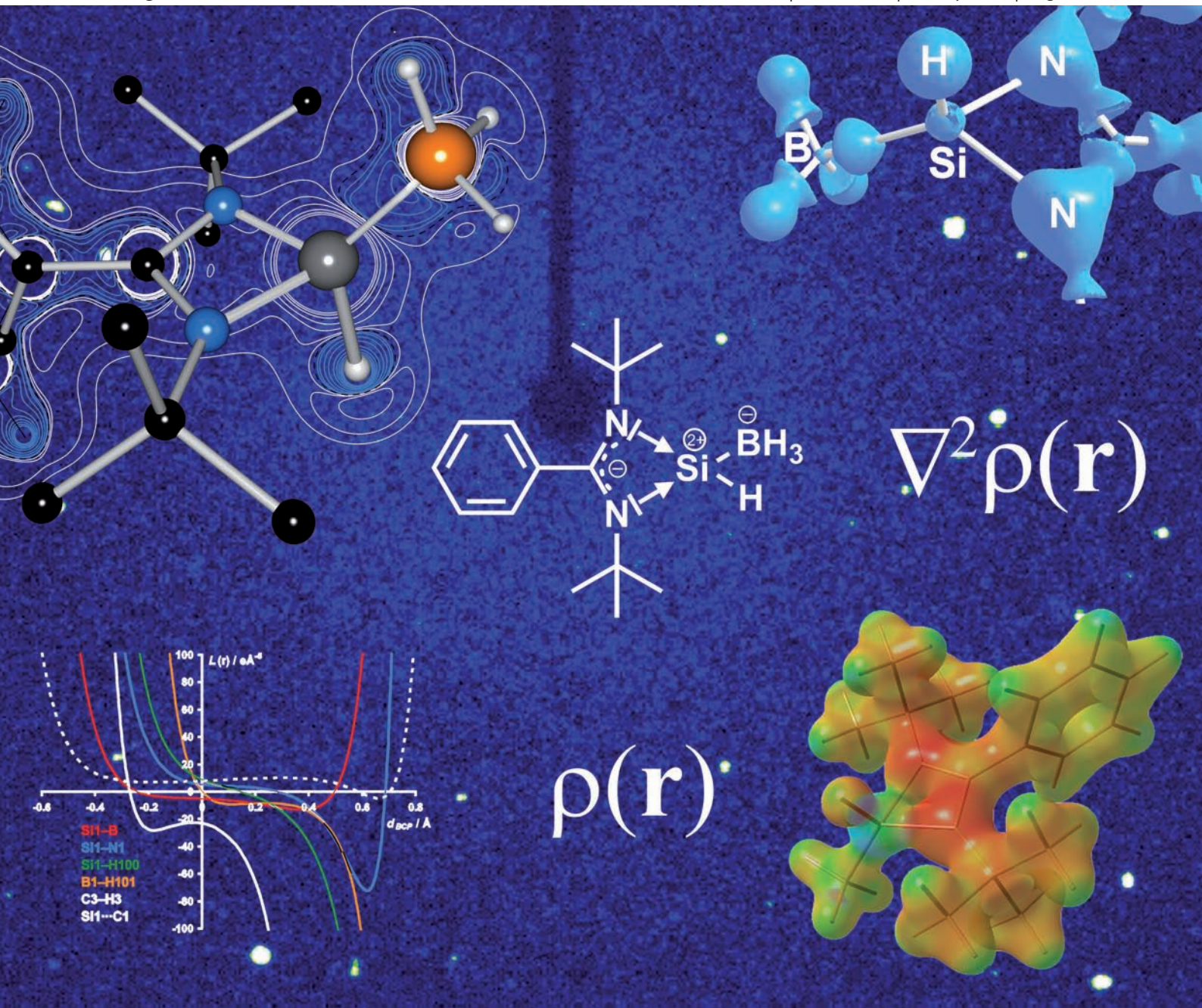


Dalton Transactions

An international journal of inorganic chemistry

www.rsc.org/dalton

Volume 40 | Number 20 | 28 May 2011 | Pages 5365–5632



ISSN 1477-9226

RSC Publishing

COVER ARTICLE
Roesky, Stalke *et al.*
A stable silicon(II) monohydride

A stable silicon(II) monohydride†‡

Anukul Jana, Dirk Leusser, Ina Objartel, Herbert W. Roesky* and Dietmar Stalke*

Received 1st December 2010, Accepted 9th March 2011

DOI: 10.1039/c0dt01675f

A stable silicon(II) monohydride is accomplished through a covalent shared interaction of the silylene lone-pair and a sp^3 -hybridized boron atom of the Lewis acidic BH_3 . Experimental charge density investigations reveal a central positively charged silicon atom bound to a negatively charged hydrogen atom. The positively charged $H-Si-BH_3$ moiety is coordinated by the lone-pairs of electrons of the benzamidinate ligand. This coordination is reinforced by a transannular $Si1 \cdots C1$ privileged exchange channel.

Introduction

The chemistry of silicon(II) dihydride has been studied at high temperature or in a matrix at very low temperatures, but it has been so far elusive at room temperature. Here we report the synthesis of a stable Lewis acid base stabilized silicon(II) monohydride, $LSiH(BH_3)$ [where L indicates $PhC(NtBu)_2$] in good yield: starting from the corresponding silicon(II) chloride, $LSiCl(BH_3)$, by the reaction with potassium K-selectride ($K[B(s-Bu)_3]H$). The ^{29}Si NMR spectrum of this compound confirms the presence of a $H-Si-BH_3$ moiety. Charge density investigations from a high-resolution low-temperature diffraction experiment reveals that there seems to be only one consistent interpretation of the electronic structure: $LSiH(BH_3)$ is the first silicon(II) monohydride, containing a central Si atom. It is stabilized through a covalent shared interaction to a sp^3 -hybridized boron atom. The positively charged $H-Si-BH_3$ moiety is coordinated by the lone-pairs of the benzamidinate ligand. These non-shared interactions allow a much more flexible coordination geometry at the silicon atom.

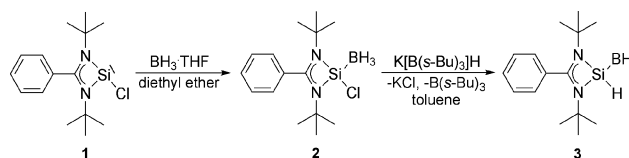
Group 14 hydrides are of practical interest as a result of their widespread use in synthetic chemistry,¹ and their employment as precursors for high purity elements as well as alloys for electronic devices.² Several hydrides are known from silicon, the sister element of carbon, derived from oxidation state +4. However, the corresponding stable silicon compound of oxidation state +2 is elusive to date. The parent member of the silylene family is silicon(II) dihydride, SiH_2 . Silylene (SiH_2) plays a central role in the field of silicon chemistry and it is considered as a transient species. It appears as the most common intermediate during decomposition reaction of silanes, which have attracted much attention because of

their importance in manufacturing amorphous silicon. The latter is used for advanced discrete electronic devices such as power transistors, and in the development of integrated circuits such as computer chips.

SiH_2 is generated for example by photolysis of phenylsilane ($PhSiH_3$) at 193 nm in the gas phase and is only stable in an argon matrix at temperatures below $-190^\circ C$.³ SiH_2 is unstable at room temperature and polymerizes or disproportionates to give insoluble products, which are of limited use. However, theoretical studies of SiH_2 ,⁴ a Lewis donor acceptor stabilized SiH_2 ,^{5a} as well as a H_3B -coordinated SiH_2 ^{5b} were carried out. Consequently, we aimed to synthesize a stable silicon(II) monohydride species at room temperature, which is important for the development of a new field in silicon chemistry.

Results and discussion

Herein, we report the syntheses (Scheme 1) of Lewis acid base stabilized monochlorosilylene, $LSiCl(BH_3)$ (**2**) and monohydrosilylene, $LSiH(BH_3)$ (**3**) by employing the chelating benzamidinate ligand L [where L indicates $PhC(NtBu)_2$].

Scheme 1 Preparation of compounds **2** and **3**.

In 2006, we reported the synthesis of a chlorosilylene, $LSiCl$ (**1**) with a stereoactive lone-pair present at the silicon atom.⁶ We tried to prepare silicon(II) hydride using compound **1**, like germanium(II) hydride and tin(II) hydride from $L'GeCl$ and $L'SnCl$ ($L' = HC(CMeNC_6H_3-iPr_2)_2$),⁷ with the reaction of K-selectride ($K[B(s-Bu)_3]H$). Unfortunately we did not obtain the expected product. Recently So *et al.* mentioned the intermediate $[PhC(NtBu)_2]SiH$, which is formed in solution.⁸ Consequently we employed the lone-pair of **1** to the Lewis acid BH_3 to yield the Lewis acid

Institut für Anorganische Chemie, Universität Göttingen, Tammannstrasse 4, 37077, Göttingen, Germany. E-mail: hroesky@gwdg.de;dstalke@chemie.uni-goettingen.de; Fax: +49-551-393373

† Electronic supplementary information (ESI) available: Details of the charge density determination. CCDC reference number 778885 for **3**. For ESI and crystallographic data in CIF or other electronic format see DOI: 10.1039/c0dt01675f

‡ Dedicated to Professor Richard F. W. Baader on the occasion of his 80th birthday.

base stabilized chlorosilylene, $\text{LSiCl}(\text{BH}_3)$ (**2**). Compound **2** was isolated as a white crystalline solid with good solubility in solvents such as diethyl ether, toluene, and THF. Furthermore, **2** is stable in solution or in the solid state at room temperature in an inert atmosphere. It has been characterized by elemental analysis and spectroscopic methods. The ^{29}Si NMR spectrum of **2** exhibits one quartet ($\delta = 46.33$ ppm), with a coupling constant of $^1J(^{29}\text{Si}-^{11}\text{B}) = 58.93$ Hz, due to the ^{11}B nucleus ($I = 3/2$). In the literature there are also reports on the synthesis of transition metal hydrides, namely iron and nickel hydride by the reaction of metal halides with potassium borohydride, $\text{K}(\text{BEt}_3)_3\text{H}$.⁹ Therefore **2** was reacted with the hydrogenating agent $\text{K}[\text{B}(\text{s-Bu})_3]\text{H}$ in toluene at -30°C to afford the stable monohydrosilylene, $\text{LSiH}(\text{BH}_3)$ (**3**) in good yield.

A solution of **3** in benzene- D_6 did not show any evidence of oligomerization or decomposition after 48 h of heating in an oil bath at 80°C . The ^1H NMR spectrum of **3** exhibits a broad resonance at $\delta = 6.12$ ppm for the Si-H proton. This NMR signal is shifted upfield when compared to that of the transition metal hydrido hydrosilylene complexes, such as $\text{Cp}^*(\text{Me}_2\text{PCH}_2\text{CH}_2\text{PMe}_2)\text{Mo}(\text{H})\text{Si}(\text{H})\text{Ph}$ ($\delta = 9.45$ ppm)^{10a} or $\text{Cp}^*(\text{CO})\text{Ru}(\text{H})\text{Si}(\text{H})\text{C}(\text{SiMe}_3)_3$ ($\delta = 9.14$ ppm)^{10b} or $\text{Cp}^*(\text{CO})_2\text{W}(\text{H})\text{Si}(\text{H})\text{C}(\text{SiMe}_3)_3$ ($\delta = 10.39$ ppm).^{10c} This was expected, because the electron density is higher at the silicon(II) atom coordinated to transition metal hydrido complexes with respect to the silicon(II) atom of monohydrosilylene, $\text{LSiH}(\text{BH}_3)$ (**3**). In the latter the lone-pair of electrons at the silicon atom coordinates to the Lewis acid BH_3 . The ^{29}Si NMR spectrum of **3** exhibits a quartet in the ^1H decoupled spectrum ($\delta = 54.31$ ppm, and $^1J(^{29}\text{Si}-^{11}\text{B}) = 56.00$ Hz) and shows a doublet of quartets in a ^1H coupled spectrum with a coupling constant of 235.12 Hz. The IR spectrum exhibits a band at 2107 cm^{-1} , which is assigned to the Si-H stretching frequency.

The central structural element of $\text{LSiH}(\text{BH}_3)$ (**3**) is a planar SiN_2C four-membered ring,¹¹ with the silicon atom basically in the plane of the chelating benzamidinate monoanionic ligand. Above and below that plane a hydride atom and the BH_3 Lewis acidic moiety is bonded to the silicon atom. The Si-H bond length of $1.47342(11)\text{ \AA}$, the Si-B distance of $1.9624(5)\text{ \AA}$, and the two equidistant Si-N distances of $1.8288(8)\text{ \AA}$ on average are in the expected range. The latter are longer than Si-N single bonds in silicon(IV) amines and represent lone-pair-driven dative $\text{N}\rightarrow\text{Si}$ bonds.¹² **3** comprises a non-crystallographic mirror plane in the CN_2Si -backbone and a two-fold axis along $\text{Si1}\cdots\text{C1}$ for the $[\text{PhC}(\text{N}t\text{Bu})_2]^-$ anion. The two tertiary carbon atoms of the $t\text{Bu}$ -substituents are only marginally out of plane. The negative charge in the benzamidinate ligand gives rise to a shortening of the N-C1 bonds to $1.339(5)\text{ \AA}$ on average, which is close to the expected value of a $\text{C}=\text{N}$ double bond (1.29 \AA). Simple geometric considerations would suggest sp^2 -hybridization for the nitrogen atoms and sp^3 -hybridization of the boron and the silicon atom. However, electron counting leads to a conflicting interpretation of the molecular structure (see Fig. 1(b)).

Therefore, the molecular structure of **3** was determined by high-resolution single crystal X-ray structure analysis (100 K , $d = 0.47\text{ \AA}$, Fig. 1(a)). Detailed insight into the bonding resulted from a multipole refinement¹³ and a subsequent topological analysis of the electron density (ED, overall experimental noise below 0.2 e\AA^{-3} to a resolution of 0.55 \AA) based on Bader's Quantum Theory of Atoms in Molecules (QTAIM).¹⁴

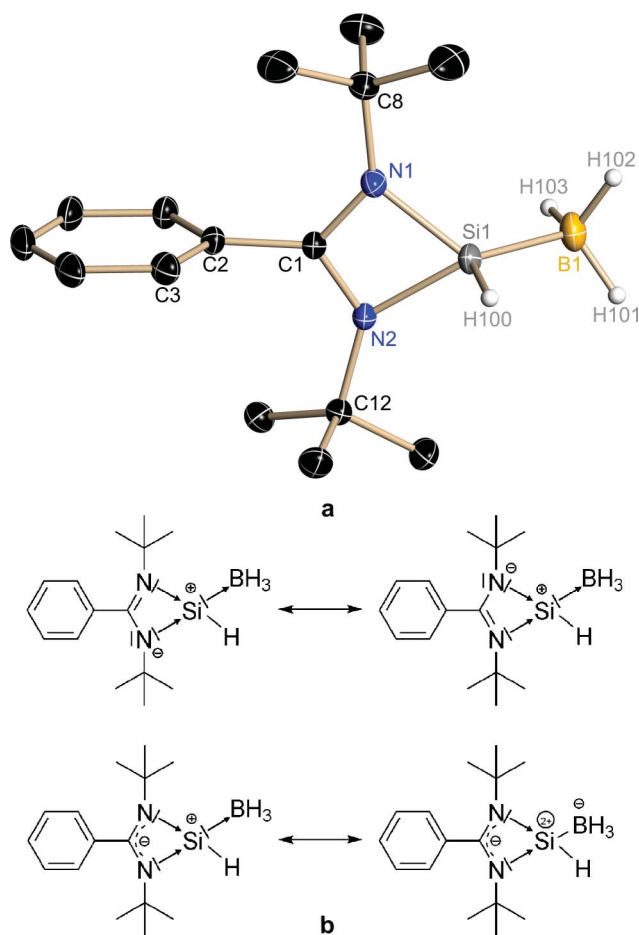


Fig. 1 (a) Molecular structure of **3** (anisotropic displacement parameters at the 50% level). Carbon bound hydrogen atoms are omitted for clarity. Displayed hydrogen atom positions have been located and refined freely and (b) Canonical Lewis diagrams of the silylene **3** emphasizing different feasible bonding modes.

Direct inspection of the ED, $\rho(\mathbf{r})$, is precluded by the huge density contributions of the core densities. Since we are interested in the fine details and changes of the ED in the vicinity of atoms (e.g. lone-pairs, valence shell polarization) and between atoms (bonding characteristics), analysis of the first (gradient field) and second derivative of the ED, the Laplacian field, $L(\mathbf{r})$, is the method of choice (see Fig. 2). Negative values of $L(\mathbf{r})$ refer to charge concentrations, while areas of positive values in the Laplacian field show charge depletions.

Analysis of the gradient leads to a characterization of bonds by the inspection of the bond path (BP), a line of maximum density between two nuclei, in terms of its length and bending, and the topological criteria at the bond critical point (BCP) (local extremum), like its position on the path relative to the two bonded atoms, the density, $\rho(\mathbf{r}_{\text{BCP}})$, the second derivative of the density, $\nabla^2\rho(\mathbf{r}_{\text{BCP}})$, and the ellipticity, $\epsilon(\mathbf{r}_{\text{BCP}})$, the ratio of the two curvatures of the density perpendicular to the bond. General rules facilitate the classification of bonds *via* the topological criteria at the BCP.¹⁵ Strength and multiple bond character rises with $\rho(\mathbf{r}_{\text{BCP}})$, negative $\nabla^2\rho(\mathbf{r}_{\text{BCP}})$ is typical for shared, positive values for closed shell interactions, non-zero ellipticity can be caused by π -contributions or coupling of lone-pair density into the bond.¹⁶

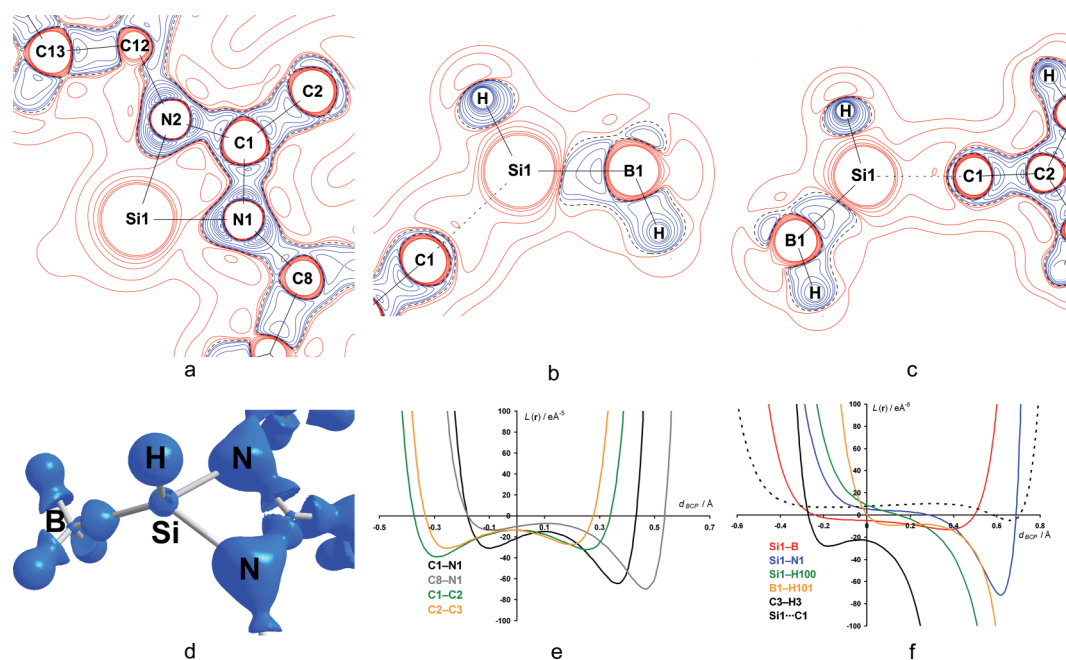


Fig. 2 $L(\mathbf{r})$ in the SiN_2^- (a), Si1, B1, H100- (b), Si1, C1, H100-plane (c), negative values ranging from -1 to $-70 \text{ e}\text{\AA}^{-5}$ (charge concentrations) are plotted in blue and positive values ranging from $+1$ to $+10 \text{ e}\text{\AA}^{-5}$ (charge depletions) in red contour lines; isosurface of $-L(\mathbf{r})$ at the $-5 \text{ e}\text{\AA}^{-5}$ level (d), plots (e) and (f) show the $L(\mathbf{r})$ along selected bond paths and the line connecting C1 and Si1 (black dotted, relative to the interatomic midpoint), with d_{BCP} being the distance from the respective BCP.

In the quantum chemical framework of QTAIM, discrete atomic volumes, the atomic basins, are defined by the zero-flux surface, given by $\nabla\rho(\mathbf{r})\cdot\mathbf{n}(\mathbf{r})$, where $\mathbf{n}(\mathbf{r})$ is the normal vector to the surface. This allows the determination of physical-based atomic charges by integration of the density over the atomic basins, providing an extremely powerful tool to judge the bonding in a molecule.

In **3** we found the typical two-dimensional Laplacian distribution for a covalent carbon-carbon and a polar nitrogen-carbon bond with the valence shell charge concentrations (VSCC) pointing towards the bonding partners (Fig. 2(a) and (c)). The analyses along the bond paths, given in Fig. 2(e) and (f), support the features for these shared covalent interactions. Shared density at both sides of the respective BCPs over a wide range in the interatomic regions is detected. The individual shape depends on the degree

of polarization. The minima of $L(\mathbf{r})$ are more pronounced for the more electronegative partner and the Laplacian is asymmetrically distributed relative to the position of the BCP. In polar bonds it is shifted away from the more electronegative bonding partner to give an increased atomic volume and charge at the expense of the more electropositive atom (also see the integrated charges in Table 1).

For the more interesting bonds, foremost those at the silicon atom, the findings are remarkable. The Si-B bond is far from a silicon-centred lone-pair driven Si \rightarrow B dative bond (Fig. 2(b) and (f)) as most of the silylene canonical forms might suggest (Fig. 1(b)). In contrast, charge is concentrated over more than 0.7 \AA in the interatomic region (Fig. 2(f)), slightly polarized towards the boron atom (Fig. 2(b) and (d)), but always negative at

Table 1 Topological parameters of the bond critical points and integrated atomic charges¹¹

	$\rho(\mathbf{r}_{\text{BCP}}) [\text{e}\text{\AA}^{-3}]$	$\nabla^2\rho(\mathbf{r}_{\text{BCP}}) [\text{e}\text{\AA}^{-5}]$	ϵ_{BCP}	$d_{\text{BP}} [\text{\AA}]$	$d1_{\text{BCP}} [\text{\AA}]$	$Q [e]$
Si-B	0.87(3)	-5.07(5)	0.10	1.966	0.983	+1.68/+1.21
Si-N1	0.83(4)	+5.17(9)	0.19	1.843	0.825	+1.68/-1.31
Si-N2	0.74(4)	+6.10(9)	0.31	1.834	0.817	+1.68/-1.20
Si-H	0.80(6)	+9.02(13)	0.50	1.480	0.776	+1.68/-0.52
N1-C8	1.75(2)	-10.21(8)	0.01	1.475	0.870	-1.31/+0.48
N1-C1	2.52(4)	-21.18(15)	0.09	1.337	0.770	-1.31/+0.60
N2-C1	2.42(3)	-17.64(13)	0.13	1.346	0.757	-1.20/+0.60
C1-C2	1.92(3)	-13.60(8)	0.09	1.483	0.755	+0.60/-0.19
C2-C3	2.06(3)	-13.84(7)	0.23	1.396	0.723	-0.19/+0.06
B-H103	1.00(2)	+1.76(6)	0.54	1.198	0.497	+1.21/-0.54
B-H101/2	0.99(1)	+0.1(4)	0.46(1)	1.22(1)	0.50(1)	+1.21/-0.54
C _{Me} -H	1.96(6)	+21(2)	0.07(4)	1.08(1)	0.64(2)	+0.03/-0.02
C _{Ph} -H	1.97(6)	+22(2)	0.05(2)	1.07(1)	0.66(1)	-0.06/+0.11

ϵ_{BCP} is the ellipticity ($\epsilon_{\text{BCP}} = \lambda_2/\lambda_1 - 1$), d_{BP} the total length of the BP, $d1_{\text{BCP}}$ the distance of the first named atom to the BCP, Q the charge of the two involved atoms, derived by the difference of atomic number Z and $\rho(\mathbf{r})$ integrated over the atomic basin.

both sides of the BCP, which supports rating the Si–B bond as a covalent interaction with shared density.

In severe contrast to this bonding mode we found the Si–H bond to be extremely polarized (Fig. 2(b), (c) and (f)). Especially when compared to the $L(\mathbf{r})$ of the other hydrogen bonds, displaying *e.g.* classical polarized but shared C–H bonds, the difference is striking. In the B–H bonds $L(\mathbf{r})$ is marginally shifted to the hydrogen-basin and the steep ascent of the Laplacian shows strong depletion as soon as the boron-basin is reached. In the Si–H bond we find concentrations solely in the vicinity of the hydrogen atom H100, which makes the distribution qualitatively more comparable to the coordinating lone-pair at the nitrogen atoms of the anionic benzamidinate ligand (Fig. 2(d)). These findings together with the huge concentration around H100 and the distinct negative charge require the classification of the silicon hydrogen bond as that of a hydride.

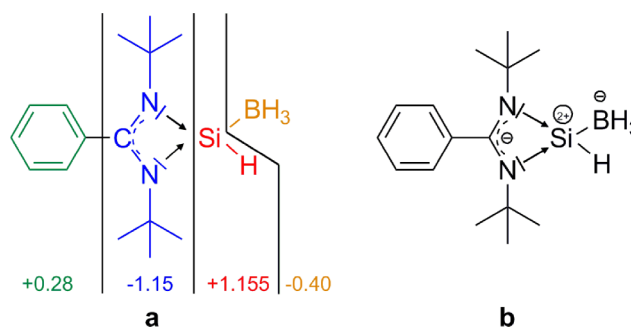
The topological analysis of the benzamidinate ligand reveals very interesting features, providing some reasoning why it is such a versatile ligand in stabilizing complexes with silicon in low oxidation state.¹⁷ The idea of the negative charge being delocalized in the N₂C1-backbone is supported by the high densities and negative Laplacians at the BCPs. Even between C1 and the *ipso* carbon atom of the phenyl ring $\rho(\mathbf{r}_{\text{BCP}})$ is higher (1.921 eÅ⁻³) than for the single bonds between the tertiary carbon atoms and the methyl groups (av.: 1.798 eÅ⁻³) and only 0.3 eÅ⁻³ below the mean value of the aromatic C–C bonds (av.: 2.231 eÅ⁻³). This is remarkable, because the phenyl ring is oriented perpendicular to the π -system of the N₂C1-unit, which precludes conjugation with the ring. More striking, however, is the presence of a flat (–5.132 eÅ⁻³) but well resolved charge concentration (CC) at C1 pointing towards the transannular silicon atom (Fig. 2(c)). This critical point in the Laplacian distribution is of the (3,+1) type and therefore different from the (3,+3) critical points (local minima of the Laplacian, respectively local maxima in the negative Laplacian distribution) found in the VSCCs of shared interactions. It is important to state that this feature is not caused by the π -density of the N₂C1-backbone, which can be easily verified by comparison with the distribution of the valence shells around the aromatic carbon atoms of the phenyl ring. However, no BP with the associated BCP could be found between C1 and Si1, even though the curvature of $L(\mathbf{r})$ along the interatomic line is akin to that of a bond.¹⁸ Although there certainly is no classical Lewis two-center-two-electron bond between Si1...C1 the interaction induced charge concentration in the valence shell at C1 might indicate a privileged exchange channel.¹⁹ Similar polarization patterns are well understood in metal–ligand interactions, where ligand induced charge concentrations at the metal atoms are described and quantified.²⁰

More prominent than this weak interaction is the ligand coordination to the electropositive silicon atom *via* the nitrogen-centered lone-pair densities. Interestingly, the extrema of the nitrogen lone-pair VSCCs are shifted away from the direct line between N and Si (Fig. 2(a)), evidence for electronic and steric strain in the molecule.²¹ The shape of the three-dimensional distribution (Fig. 2(d)) is not typical for a well defined sp²-lone-pair. The isosurface representation of a single free or coordinating lone-pair is generally formed like a convex plate.²² The distribution in **3** is leaping out perpendicular to the SiN₂-plane, reminiscent to oxygen atoms, where two lone-pairs merge to one broad VSCC.²³

This spatial distribution fits a hybridization state half way between sp² and sp³ at the nitrogen atoms. $L(\mathbf{r})$ is negative close to the nitrogen atom due to the charge concentration caused by the coordinating lone-pair (extremum of the VSCC about 0.4 Å from the core) but the concentration is not reaching out far. Already 0.3 Å ahead of the BCP, $L(\mathbf{r})$ turns positive, hence to charge depletion and stays positive for the whole bond path until reaching the inner core of the silicon atom (Fig. 2(a) and (f)). This is the typical shape found for dative or ionic bonds. There is no shared density to give rise to an interatomic charge concentration and there is not much difference in $L(\mathbf{r})$ along the BP between the Si–N bonds and the Si–H100 bond. The shape of the basin around silicon in the direction of the ligand and H100 is that of an ion: distinct and spherical charge depletion. The silicon atom seems to have two faces in **3**: covalent towards boron and closed shell towards the benzamidinate ligand and the hydride H100.

We found four VSCCs around the boron atom B1 which form almost ideal tetrahedral angles between 108.7° and 110.7°, in contrast to the classical bond angles from straight interatomic lines. Those range from 100.9° to 116.4° in a quite unsystematic appearance. Similarly, looking at the angles between the VSCCs at the carbon atom C1 as well provides a more consistent picture than referring to the classically quoted bond angles: 126.2° (CC_{N1}–CC_{C1}–CC_{N2}), 114.8°, and 118.9° (CC_{C2}–CC_{C1}–CC_{N1/N2}) vs. 106.24(3)° (N1–C1–N2), 128.16(3)° (N1–C1–C2), 125.59(3)° (N2–C1–C2), respectively.

Conclusive evidence for the electronic interpretation of **3** as the first Si(II)-hydride was gained by integration of all symmetry independent atomic basins. In Table 1 the atomic charges display prominent positive values for silicon (+1.68 e), boron (+1.21 e), and even C1 (+0.60 e), mainly counterbalanced by N1 (–1.31 e), N2 (–1.21 e), and the hydrogen atoms bound to silicon (–0.53 e) and boron (av.: –0.53 e). Even more meaningful are the group charges, which are displayed in Scheme 2a.



Scheme 2 (a) Group charges in **3** gained from the integration of atomic basins as sum over the integrated atomic charges and (b) canonical formula that contributes most to explain the bonding.

From there the intramolecular charge transfer is obvious. Even the BH₃ group bears negative charge. The positive charge at the boron atom itself is overcompensated by the negative hydrogen atoms. As expected, we found a neutral phenyl ring and the whole negative charge of the ligand to be concentrated in the C(NtBu)-backbone. Surprisingly, it is exclusively accumulated in the nitrogen basins while the C1-basin gains positive charge, because the electronegative nitrogen atoms polarize the C–N bonding density.

In addition, the hydride atom H100 counterbalances in part the positive charge at Si1, but the SiH-core remains positive.

Experimental section

General considerations

All manipulations were performed in a dry and oxygen-free N₂ atmosphere by using Schlenk-line and M-Braun MB 150-GI glove-box techniques. Solvents were purified with the M-Braun solvent drying system. The ¹H, ¹¹B, ¹³C, and ²⁹Si NMR spectra were recorded on a Bruker Avance DRX 500 MHz spectrometer and referenced to the deuterated solvent in the case of the ¹H and ¹³C, BF₃·OEt₂ for ¹¹B, and SiMe₄ for ²⁹Si used as reference. EI-MS were measured on a Finnigan Mat 8230 instrument. Elemental analyses were performed by the Analytisches Labor des Instituts für Anorganische Chemie der Universität Göttingen. Infrared spectral data were recorded on a Perkin–Elmer PE-1430 instrument. Melting points were measured in sealed glass tubes with a Büchi B 540 melting point instrument. Benzene-D₆ was dried by distillation after drying with potassium under reflux in the presence of benzophenone. All commercially available compounds (Aldrich, Across) were used as received unless stated otherwise. The starting material LSiCl (**1**) was synthesized according to the literature procedure.¹⁷

Synthesis of LSiCl(BH₃) (2**).** BH₃·THF (2 mL, 1 M, 2 mmol) was added to a toluene solution (35 mL) of **1** (0.59 g, 2 mmol) at –30 °C. The reaction mixture was allowed to warm slowly to room temperature and stirred further for 1 h at this temperature. After that all the volatiles were removed in a vacuum. The residue was dissolved in toluene (40 mL), and the solution was filtered over celite. The resulting solution was concentrated (to about 20 mL), and was stored overnight in a freezer at –30 °C to afford colorless crystals (0.49 g, 80% yield). Mp: 242 °C. ¹H NMR (C₆D₆, 500 MHz): δ 1.02 (s, 18H, C(CH₃)₃), 1.39 (q, *J* = 93.95 Hz, 3H, BH₃), 6.70–6.93 (m, 5H, C₆H₅) ppm. ¹¹B NMR (C₆D₆, 160 MHz): δ –41.96 ppm. ¹³C NMR (C₆D₆, 125 MHz): δ 30.75 (C(CH₃)₃), 55.24 (C(CH₃)₃), 127.49, 128.08, 128.25, 128.32, 129.63, 130.87 (C₆H₅), 174.93 (NCN) ppm. ²⁹Si NMR (C₆D₆, 99 MHz): δ 46.33 (q, *J*(²⁹Si–¹¹B) = 58.93 Hz) ppm. EI-MS (70 eV): *m/z* (%): 294 (100) [M⁺ – BH₃]. Anal. calcd for C₁₅H₂₆BClN₂Si (308.16): C, 58.36; H, 8.49; N, 9.07. Found C, 58.15; H, 8.95; N, 8.65.

Synthesis of LSiH(BH₃) (3**).** A solution of K[B(*s*-Bu)₃]H in THF (2 mL, 1 M, in THF) was slowly added drop by drop to a stirred solution of **2** (0.61 g, 2 mmol) in toluene (30 mL) at –30 °C. The reaction mixture was warmed to room temperature and stirred for an additional 2 h. After removal of all the volatiles, the residue was extracted with toluene (20 mL) to yield colorless compound **3**. Suitable crystals for single crystal X-ray structural analysis were obtained from a saturated hot *n*-hexane solution (0.35 g, 65%). Mp: 182 °C. ¹H NMR (C₆D₆, 500 MHz): δ 1.00 (s, 18H, C(CH₃)₃), 1.28 (q, *J* = 92.38 Hz, 3H, BH₃), 6.12 (br, 1H, SiH), 6.77–6.91 (m, 5H, C₆H₅) ppm. ¹¹B NMR (C₆D₆, 160 MHz): δ –42.88 ppm. ¹³C NMR (C₆D₆, 125 MHz): δ 30.84 (C(CH₃)₃), 54.12 (C(CH₃)₃), 127.91, 128.29, 128.32, 128.38, 130.51, 131.34 (C₆H₅), 170.85 (NCN) ppm. ²⁹Si NMR (C₆D₆, 99 MHz): δ 54.31 (*J*(²⁹Si–¹H) = 235.12 Hz and *J*(²⁹Si–¹¹B) = 56.00 Hz) ppm. IR (Nujol, KBr): $\tilde{\nu}$ = 2107 cm^{–1} (Si–H). EI-MS (70 eV): *m/z* (%): 260

(100) [M⁺ – BH₃]. Anal. calcd for C₁₅H₂₆BN₂Si (274.20): C, 65.68; H, 9.92; N, 10.21. Found C, 64.92; H, 9.86; N, 10.12.

Crystallographic details for **3.** The high-resolution data for the multipole refinement were collected from an oil-coated shock-cooled crystal²⁴ on a BRUKER TXS diffractometer with D8 goniometer and INCOATEC Helios mirror optics (Mo-K α radiation, λ = 0.71073 Å) equipped with an open stream liquid nitrogen cooling device and an APEXII detector. The data for the multipole refinement were collected in an omega-scan mode ($\Delta\omega$ = 0.3°) at fixed ϕ -angles with a detector distance of 5 cm (low and mid-order data) and 4 cm (high-order data) at exposure times between 10 (low-order) and 180 s (high-order data). This procedure led to a high-resolution data set (for details see ESI, Table S1†), which was corrected for absorption, scaled and merged with SADABS-2008/2.²⁵

The structure was solved with SHELXS,²⁶ and a conventional Independent Atom Model (IAM) refinement using all data was performed with SHELXL²⁷ to check the data quality and to determine the absolute structure. The refined IAM served as the starting model for the subsequent multipole refinement.

The following strategy was applied: the positional and anisotropic displacement parameters of the non-hydrogen atoms were refined with the high-order data (d_{\max} = 0.60 Å). These parameters were kept fixed during the subsequent refinement steps. The hydrogen atoms were identified by a difference Fourier analysis using the low-order data (d_{\min} = 1.00 Å). Based on the same subset of data, the hydrogen atom positions were refined with a SADI-restraint for the boron-bound hydrogen atoms and an isotropic riding model (default values of SHELXL) for the sp³- (methyl, BH₃) and sp²-bound hydrogen atoms was applied. Then the hydrogen atoms were shifted along their bonding vectors to distances of 1.085 Å for those bound to sp³-hybridized carbon atoms, 1.076 Å for those bound to sp²-hybridized carbon atoms, 1.200 Å for the BH₃, and 1.480 Å for H100, which is bonded to the silicon atom.^{28,29}

Multipole refinement. The multipole refinement using the atom-centered multipole model of Hansen and Coppens³⁰ was carried out on *F*² with the full-matrix-least-squares refinement program XDLSM implemented in the XD2006³¹ program package. The core and the spherical valence densities were composed of relativistic Dirac–Fock wave functions reported by Su, Coppens and Macchi (SCM bank file).³² Single-zeta orbitals with energy-optimized Slater exponents were used for the deformation density terms.³³ The radial fit of these functions was optimized by refinement of the expansion-contraction parameters κ and κ' . The expansions over the spherical harmonics were truncated at the hexadecapolar level for all heteroatoms and all multipoles (n_l = 1 to 4) of each atom shared the same κ' -set. The deformation densities of the hydrogen atoms were represented by bond directed dipoles and quadrupoles. To derive adequate parameters for the contraction of the hydrogen atoms, κ and κ' values suggested by Volkov *et al.* were introduced and kept fixed during the refinement.³⁴ In the final cycles all parameters except κ' were refined together using all positive reflections (no *I*/ σ exclusion to avoid bias) until convergence was reached. Several chemical and non-crystallographic symmetry constraints were applied (details are given in the ESI†). The electron density is not biased by and is well separated from the thermal motion of the non-hydrogen

atoms. This was justified by the rigid bond test (DMSDA test) according to Hirshfeld.³⁵

Crystallographic data for compound 3. C₁₅H₂₇BN₂Si, *M* = 274.29 g mol⁻¹, *T* = 100(2) K, orthorhombic, space group *P*2₁2₁2₁, *a* = 8.516(2), *b* = 11.588(3), *c* = 17.098(5) Å, *V* = 1687.2(8) Å³, *Z* = 4, ρ_{calc.} = 1.080 Mg m⁻³, μ = 0.129 mm⁻¹, *F*(000) = 600, 86 541 reflections measured, 15 218 independent (*R*(int) = 0.0253), *R*1 (all data) = 0.0320, *R*2 (all data) = 0.0399, Flack parameter: 0.01(4).

Conclusion

Conclusively, there seems to be only one consistent interpretation of the electronic structure. **3** is the first silicon(II) monohydride, containing a Si^{1.68+} central atom (Scheme 2b). It is stabilized through a covalent shared interaction to a sp³-hybridized boron atom of the Lewis acid BH₃. The positively charged H–Si–BH₃ moiety is coordinated by the lone-pairs of the benzamidate ligand. The orientation of the VSCCs associated with those lone-pair densities seem to be first of all caused by hybridization requirements and not by a directed shared interaction with the silicon atom. Non-shared interactions allow a much more flexible coordination response of the ligand at the silicon atom since the bonding is not predominantly orbital-controlled. We conclude that the interaction between the silicon atom and the ligand is mainly of a closed shell non-covalent N-lone-pair character, reinforced by a transannular Si1...C1 privileged exchange channel. The negative charge of the ligand is spread over the C1N₂-backbone by a merge of two extreme electronic situations: either in a π-system formed by p-orbitals perpendicular to the sp²-hybridized atoms C1, N1, and N2, or lone-pair density coupling back into the C1N₂-unit of the two negatively charged sp³-hybridized nitrogen atoms. However, the density is distinctly polarized, leading to a negative charge at the nitrogen atoms, which counterbalances the positive silicon(II) hydride by an interaction of the closed shell type.

Acknowledgements

We are grateful to the Deutsche Forschungsgemeinschaft, in particular to the DFG Priority Program 1178 *Experimental charge density as the key to understand chemical interactions* and the DNRf funded Center of Materials Crystallography, Aarhus.

References

- 1 W. P. Neumann, *Synthesis*, 1987, 665–683.
- 2 J. G. Ekerdt, Y.-M. Sun, A. Szabo, G. J. Szulcowski and J. M. White, *Chem. Rev.*, 1996, **96**, 1499–1517.
- 3 C. Yamada, H. Kanamori, E. Hirota, N. Nishiwaki, N. Itabashi, K. Kato and T. Goto, *J. Chem. Phys.*, 1989, **91**, 4582–4586.
- 4 G. Trinquier, *J. Am. Chem. Soc.*, 1990, **112**, 2130–2137.
- 5 (a) P. V. Bharatam, R. Moudgil and D. Kaur, *Organometallics*, 2002, **21**, 3683–3690; (b) P. V. Bharatam, R. Moudgil and D. Kaur, *Inorg. Chem.*, 2003, **42**, 4743–4749.

- 6 C.-W. So, H. W. Roesky, J. Magull and R. B. Oswald, *Angew. Chem.*, 2006, **118**, 4052–4054, (*Angew. Chem., Int. Ed.*, 2006, **45**, 3948–3950).
- 7 (a) A. Jana, D. Ghoshal, H. W. Roesky, I. Objartel, G. Schwab and D. Stalke, *J. Am. Chem. Soc.*, 2009, **131**, 1288–1293; (b) A. Jana, H. W. Roesky, C. Schulzke and A. Döring, *Angew. Chem.*, 2009, **121**, 1126–1129, (*Angew. Chem., Int. Ed.*, 2009, **48**, 1106–1109).
- 8 S.-H. Zhang, H.-X. Yeong, H.-W. Xi, K. H. Lim and C.-W. So, *Chem.–Eur. J.*, 2010, **16**, 10250–10254.
- 9 (a) J. M. Smith, R. J. Lachicotte and P. L. Holland, *J. Am. Chem. Soc.*, 2003, **125**, 15752–15753; (b) S. Pfirrmann, C. Limberg and B. Zeimer, *Dalton Trans.*, 2008, 6689–6691.
- 10 (a) B. V. Mork, T. D. Tilley, A. J. Schultz and J. Cowan, *J. Am. Chem. Soc.*, 2004, **126**, 10428–10440; (b) M. Ochiai, H. Hashimoto and H. Tobita, *Angew. Chem.*, 2007, **119**, 8340–8342, (*Angew. Chem., Int. Ed.*, 2007, **46**, 8192–8194); (c) T. Watanabe, H. Hashimoto and H. Tobita, *Angew. Chem.*, 2004, **116**, 220–223, (*Angew. Chem., Int. Ed.*, 2004, **43**, 218–221).
- 11 Details of the charge density determination are available in the ESI for this article and from the CCDC (778885).
- 12 N. Kocher, J. Henn, B. Gostevskii, D. Kost, I. Kalikhman, B. Engels and D. Stalke, *J. Am. Chem. Soc.*, 2004, **126**, 5563–5568.
- 13 A. Volkov, P. Macchi, L. J. Farrugia, C. Gatti, P. R. Mallinson, T. Richter and T. Koritsanzky, XD2006, 2006.
- 14 R. F. W. Bader, *Atoms in Molecules – A Quantum Theory*, Oxford University Press, New York, USA, 1990.
- 15 T. S. Koritsanzky and P. Coppens, *Chem. Rev.*, 2001, **101**, 1583–1627.
- 16 D. Leusser, J. Henn, N. Kocher, B. Engels and D. Stalke, *J. Am. Chem. Soc.*, 2004, **126**, 1781–1793.
- 17 S. S. Sen, H. W. Roesky, D. Stern, J. Henn and D. Stalke, *J. Am. Chem. Soc.*, 2010, **132**, 1123–1126.
- 18 R. F. W. Bader, *J. Phys. Chem. A*, 2009, **113**, 10391–10396.
- 19 A. M. Pendás, E. Francisco, M. A. Blanco and C. Gatti, *Chem.–Eur. J.*, 2007, **13**, 9362–9371.
- 20 P. Roquette, A. Mwqaronna, A. Peters, E. Kaifer, H.-J. Himmel, C. Hauf, V. Herz, E.-W. Scheidt and W. Scherer, *Chem.–Eur. J.*, 2010, **16**, 1336–1350.
- 21 S. Deuerlein, D. Leusser, U. Flierler, H. Ott and D. Stalke, *Organometallics*, 2008, **27**, 2306–2315.
- 22 H. Ott, U. Pieper, D. Leusser, U. Flierler, J. Henn and D. Stalke, *Angew. Chem.*, 2009, **121**, 3022–3026, (*Angew. Chem., Int. Ed.*, 2009, **48**, 2978–2982).
- 23 N. Kocher, D. Leusser, A. Murso and D. Stalke, *Chem.–Eur. J.*, 2004, **10**, 3622–3631.
- 24 (a) T. Kottke and D. Stalke, *J. Appl. Crystallogr.*, 1993, **26**, 615–619; (b) T. Kottke, R. J. Lagow and D. Stalke, *J. Appl. Crystallogr.*, 1996, **29**, 465–468; (c) D. Stalke, *Chem. Soc. Rev.*, 1998, **27**, 171–178.
- 25 G. M. Sheldrick, *SADABS 2006/3*, Göttingen, Germany, 2006.
- 26 G. M. Sheldrick, *SHELXS* in *SHELXTL v6.10*, Madison, USA, 2001.
- 27 G. M. Sheldrick, *SHELXL* in *SHELXTL v6.10*, Madison, USA, 2001.
- 28 F. H. Allen, *Acta Crystallogr., Sect. B: Struct. Sci.*, 1986, **42**, 515–522.
- 29 P. Rademacher, *Strukturen organischer Moleküle*, VCH, Weinheim/New York, 1987.
- 30 N. K. Hansen and P. Coppens, *Acta Crystallogr., Sect. A: Cryst. Phys., Diffr., Theor. Gen. Crystallogr.*, 1978, **34**, 909–921.
- 31 A. Volkov, P. Macchi, L. J. Farrugia, C. Gatti, P. R. Mallinson, T. Richter and T. Koritsanzky, XD2006, A Computer Program Package for Multipole Refinement, Topological Analysis of Charge Densities and Evaluation of Intermolecular Energies from Experimental or Theoretical Structure Factors, 2006.
- 32 (a) Z. Su and P. Coppens, *Acta Crystallogr., Sect. A: Found. Crystallogr.*, 1998, **54**, 646–652; (b) P. Macchi and P. Coppens, *Acta Crystallogr., Sect. A: Found. Crystallogr.*, 2001, **57**, 656–662.
- 33 (a) E. Clementi and D. L. Raimondi, *J. Chem. Phys.*, 1963, **38**, 2686–2689; (b) E. Clementi and C. Roetti, *At. Data Nucl. Data Tables*, 1974, **14**, 177–478.
- 34 A. Volkov, Y. A. Abramov and P. Coppens, *Acta Crystallogr., Sect. A: Found. Crystallogr.*, 2001, **57**, 272–282.
- 35 F. L. Hirshfeld, *Acta Crystallogr., Sect. A: Cryst. Phys., Diffr., Theor. Gen. Crystallogr.*, 1976, **32**, 239–244.